ORIGINAL PAPER



Investigation of direction- and age-dependent prestretch in mouse cranial dura mater

Jack Consolini¹ · Alyssa G. Oberman² · John Sayut¹ · Frederick W. Damen³ · Craig J. Goergen³ · Matthew J. Ravosa² · Maria A. Holland^{1,4}

Received: 5 July 2023 / Accepted: 30 November 2023 © The Author(s), under exclusive licence to Springer-Verlag GmbH Germany, part of Springer Nature 2024

Abstract

Cranial dura mater is a dense interwoven vascularized connective tissue that helps regulate neurocranial remodeling by responding to strains from the growing brain. Previous ex vivo experimentation has failed to account for the role of prestretch in the mechanical behavior of the dura. Here we aim to estimate the prestretch in mouse cranial dura mater and determine its dependency on direction and age. We performed transverse and longitudinal incisions in parietal dura excised from newborn (day ~4) and mature (12 weeks) mice and calculated the ex vivo normalized incision opening (measured width over length). Then, similar incisions were simulated under isotropic stretching within Abaqus/Standard. Finally, prestretch was estimated by comparing the ex vivo and in silico normalized openings. There were no significant differences between the neonatal and adult mice when comparing cuts in the same direction, but adult mice were found to have significantly greater stretch in the anterior–posterior direction than in the medial–lateral direction, while neonatal dura was essentially isotropic. Additionally, our simulations show that increasing curvature impacts the incision opening, indicating that flat in silico models may overestimate prestretch.

Keywords Mouse · Cranial dura mater · Prestretch · Finite element method

1 Introduction

Scientific and clinical research on mammalian brain and skull development provide evidence that the cranium expands concurrently with the growing brain. Pressure from the developing brain fosters morphological modeling and remodeling of the cranial vault by inducing quasi-static tensile strains within the cranial sutures. This leads to mineralization of the fibrous joints of the cranial vault via intramembranous ossification and cartilaginous joints of the cranial

Maria A. Holland maria-holland@nd.edu

Published online: 11 January 2024

- Department of Aerospace and Mechanical Engineering, University of Notre Dame, Notre Dame, IN 46556, USA
- ² Center for Functional Anatomy and Evolution, Johns Hopkins University School of Medicine, Baltimore, MD 21205, USA
- Weldon School of Biomedical Engineering, Purdue University, West Lafayette, IN 47907, USA
- Bioengineering Graduate Program, University of Notre Dame, Notre Dame, IN 46556, USA

base via endochondral ossification (Liu et al. 2011; Richtsmeier and Flaherty 2013; Weickenmeier et al. 2017; Weiss-Bilka et al. 2018). The dura mater, the outermost meningeal tissue fixed to the calvarium, appears to act as a very important mechanoreceptor and mechanotransmitter for properly timed and paced cranial suture closure (Fabris et al. 2019; Gagan et al. 2007; Jaslow 1990; Ogle et al. 2004; Liu et al. 2011). The collagenic bilayered dura contains fibroblasts and osteoblasts in its periosteal (outer) layer, which migrate to the suture site once mineralization has begun (Gagan et al. 2007; McGarvey et al. 1984; Vandenabeele et al. 1996; Suh 2020). The dura mater must correctly respond to pressure from the growing brain, as an improper reaction can lead to premature release of bone-producing cells and growth factors (Fong et al. 2003; Greenwald et al. 2000; Richtsmeier and Flaherty 2013).

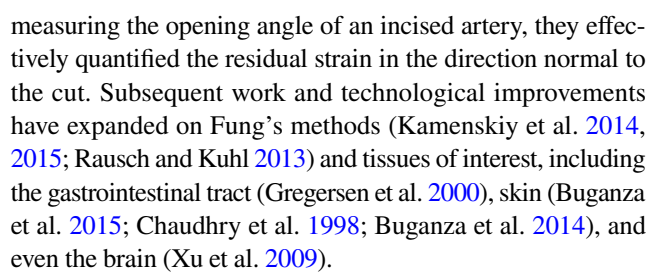
The dura mater's material composition (e.g., thickness and collagen structure) and mechanical properties (e.g., strength, stiffness, elasticity, and permeability) influence how the tissue senses strain. Prior work has shown that absence of cranial dura mater (Opperman et al. 1995) and modifications in the dura's mechanical properties (Fong



et al. 2003; Greenwald et al. 2000) lead to cranial malformations, which have been attributed to alterations in cytokine expression and osteoblastic differentiation. Fortunately, cranial malformations, known as craniosynostoses, can be effectively resolved with surgical intervention and dural grafts (Aydin et al. 2011; Borghi et al. 2018; Yu et al. 2021). Safety and efficacy of the procedures strongly rely on the dura remaining intact, for tearing could lead to vascular leakage or infection (Aydin et al. 2011). Dural incisions are unavoidable for more invasive neurosurgical procedures, making postoperative cerebrospinal fluid leak a prevalent complication associated with improper dural tissue repair or reconstruction (Becker et al. 2003). Understanding dural anatomy and mechanics is key here, as attempting to graft tissue requires the creation of watertight sutures without tearing the existing tissue (Abuzayed et al. 2009) and consideration for how the area needs to remain vascularized throughout healing (Yamaki et al. 1991). Thus, effective growth pathology correction and dural repair require better characterization of the dura mater's in vivo structure, mechanical strength, and material behavior.

It is understood that mammalian (human, pig, and rat) dura mater deforms non-linearly (Bylski et al. 1986; Fong et al. 2003; Kriewall et al. 1983; Maikos et al. 2008; Melvin et al. 1970; Pierrat et al. 2020; Zwirner et al. 2019) and viscoelastically (Henderson et al. 2005; Maikos et al. 2008; Melvin et al. 1970; Shulyakov et al. 2011). Cranial dura also appears to be globally isotropic (Kriewall et al. 1983; Wolfinbarger et al. 1994), however, observed variations in thickness (Fam et al. 2018; Kuchiwaki et al. 1997; Patin et al. 1993) and collagen alignment/structure (McGarvey et al. 1984; Protasoni et al. 2011; Vandenabeele et al. 1996; Wolfinbarger et al. 1994), indicate that it may be locally heterogeneous and anisotropic. The majority of the dura's mechanical characterization has come from uniaxial (Aydin et al. 2019; Maikos et al. 2008; Noort et al. 1981; Wolfinbarger et al. 1994; Zwirner et al. 2019; Pierrat et al. 2020) and biaxial (Bylski et al. 1986; Kriewall et al. 1983; Pierrat et al. 2020) tensile tests on freshly excised or preserved samples with simple geometries (typically dumbbell, rectangle, or square). Unfortunately, these ex vivo experiments fail to capture important characteristics of the dura mater's in situ environment, such as the impact of the tissue's curvature or firm connection to the skull. Moreover, aside from generic pre-conditioning done prior to loading, almost all studies neglect to consider the residual strain or prestretch the dura mater experiences in vivo.

While prestretch has not been deeply studied in the case of cranial dura mater, the study of residual strains and stresses has been heavily reported on within the broader field of tissue mechanics. The classical procedure for investigating residual strain was instituted by Fung and Liu (1989) and Han and Fung (1991), who performed cut experiments into arterial tissue. By



A principal through-line of these works is the indication of inconsistencies between ex vivo and in vivo measurements (Rausch and Kuhl 2013). Ex vivo tissue is loaded from zero strain, where the collagen fibrils maybe be significantly curled and crimped, while the collagen fibrils of many in vivo tissues are already relatively taut under prestretch. Thus, under a given load, the measured strains ex vivo are generally larger than in vivo estimations (Rausch and Kuhl 2013). Additionally, in nonlinear tissues, prestretch places the tissue out of their linear toe region and into a stiffer regime. Because of this, ex vivo measurements tend to underestimate tissue stiffness (Rausch and Kuhl 2013). Furthermore, the measured stiffnesses could be affected by the ex vivo conditions, with excised tissue often being softer and more brittle (McGarvey et al. 1984).

Along with minimally invasive procedures, computational models have been used to bridge the gap between ex vivo and in vivo measurement discrepancies. Recent research (Henderson et al. 2005; Rausch and Kuhl 2013) has demonstrated how effective finite element analyzes can be for the characterization of prestretch, and have inspired the current work. Here, we aimed to build upon an earlier investigation of the direction- and age-dependency of residual strain present in cranial dura mater (Henderson et al. 2005). Specifically, we estimated prestretch with a more realistic three-dimensional finite element model, adopting a mathematical model of finite strain to numerically simulate prestretch (Rausch and Kuhl 2013). First, we performed incisions within excised neonatal and adult mice dura mater and calculated the normalized incision openings (measured width over length). Next, we created finite element models of incisions in ellipsoidal geometries of prestretched dura mater. Then, we consider the effects of different modeling and experimental choices, namely the incision length and curvature on normalized opening. Finally, we estimated the prestretch in both transverse and longitudinal directions in the neonatal and adult mice, as well as the growth deformation that takes place between those two timepoints.

2 Methods

2.1 Animal experiments

ICR (Institute of Cancer Research) mice were purchased from Envigo (Indianapolis, IN) for all studies. Male and



female time-dated (4–20 weeks) mice were used for in vivo Magnetic Resonance (MR) imaging and segmentation, while 12-week pregnant mice were obtained for ex vivo experimentation. All animal experiments were performed in accordance with the Institutional Animal Care and Use Committees (IACUC) at the respective institutions.

2.1.1 In vivo MR imaging and segmentation

To quantify the deformation of neural tissues during normal cranial development, we captured MR images of male (n=3) and female (n=3) ICR mice every 4 weeks for 20 weeks (Fig. 1). All imaging experiments were performed in accordance with the IACUC at Purdue University (protocol #2002002016). Volumetric imaging data was acquired on a 7T MRI scanner (Bruker BioSpin MRI) in the Purdue MRI facility using a 3D FLASH T1-weighted sequence (TE/TR = 4.97/50 ms; FA = 20 deg; matrix size = 180×180 ; FOV: 18×18 mm; slice thickness = 0.1 mm; NEX: 2). During post-processing of acquired data, one image from week 8 was excluded from further analysis due to poor image quality.

Brain scans were processed using the FMRIB (Functional Magnetic Resonance Imaging of the Brain) Software Toolkit, or FSL (Woolrich et al. 2009). Existing segmentation methods for human brains could not be applied due to the mouse's smaller, differently shaped brain, necessitating a semi-automated segmentation process. We first performed a manual slice-by-slice removal of some of the surrounding tissue, including the olfactory bulb, followed by an automated identification of the brain tissue using FSL (Fig. 2). The surface area of the brain, used as a proxy for the surface area of the dura mater, was calculated through FSL.

2.1.2 Ex vivo dural incisions

Pregnant females were housed and fed for roughly five days in a temperature- and light-controlled environment. Upon birth of the pups—normally a day after the mice were received—the newborn mice were housed with the adult

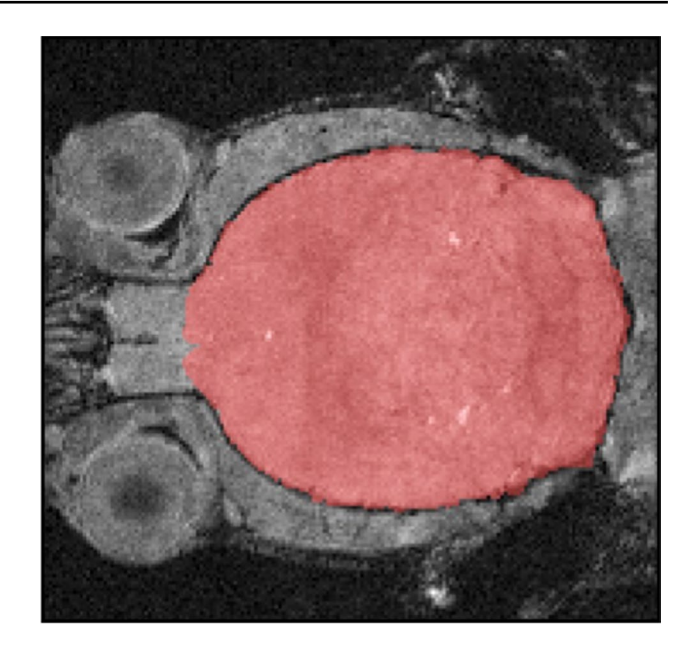


Fig. 2 Resulting segmentation of 16-week-old female mouse brain from in vivo MRI scan slice. Some tissue surrounding the brain was manually removed to expand the space between the brain and skull, after which FSL automatically identifies the brain tissue and creates a mask (shown in red)

females. Four days after birth, the adult mice were sacrificed via CO₂ inhalation using a Euthanex chamber (Fig. 1). The neonatal mice were sacrificed via decapitation after being anesthetized in a bell jar with isoflourane. Within three hours of sacrifice, the head was separated from the body and the cranium and dura mater were dissected by removing the skin, cutting the skull open along the lower jaw line, removing the nasal bone, and carefully removing the brain (Fig. 3). This left the dura mater intact along the frontal, parietal, and occipital bones of the cranial vault. It was important that the dura mater was not scraped off of the interior skull, as the adhesion to the skull maintained the dura's stretched configuration, even once the mouse was deceased. Additional tissue was stripped away to avoid obscuring the cut area along the calvaria.

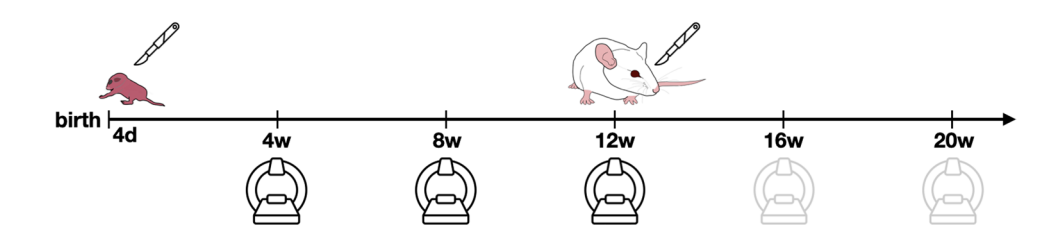


Fig. 1 Timeline of mice ages used for ex vivo and in vivo experiments. The ex vivo dural incisions were performed at 4 days and 12 weeks of maturity. In vivo imaging was conducted between weeks 4 and 20, indicated by the MR machine schematic. Note that weeks

16 and 20 have been grayed out because they are not included in our growth analyzes (Sect. 3.6) in order to make the best comparison with our ex vivo data



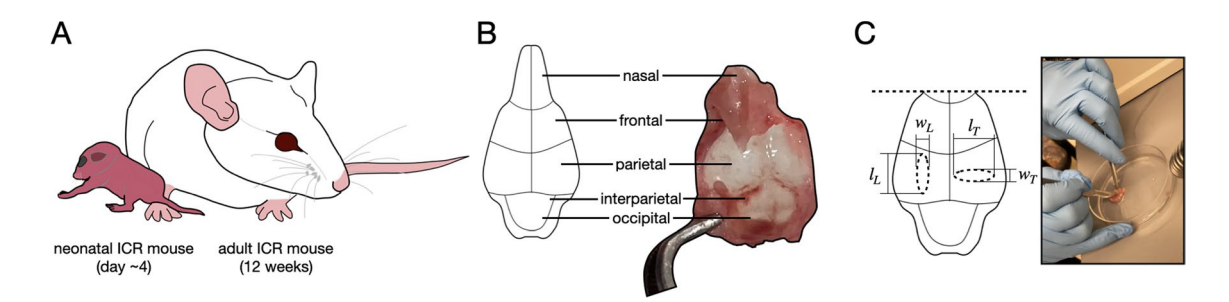


Fig. 3 Procedure for ex vivo dural incision on neonatal and adult mouse cranial dura mater. **A** Pregnant adult female ICR mice (12 weeks) were housed until giving birth to mice pups. **B** On postpartum day four, the two age groups were sacrificed, with their cranium and dura mater dissected within three hours of sacrifice. Care was taken

to extract the dura mater intact with the calvaria, to capture the in situ conditions. C Transverse and longitudinal cuts were made within in dura mater overlying the parietal lobes. Images were taken immediately after and five minutes later

A no. 11 blade scalpel was used to incise the dissected dura mater while immersed in phosphate buffer saline (PBS). With the skull positioned with the dura mater facing up, we made longitudinal (anterior–posterior) and transverse (medial–lateral) incisions, attempting to keep the incisions within the middle of the parietal dura. Despite attempting to make uniformly sized incisions, the manual location of the middle point and the extremely small size led to significant deviations in cut sizes and locations. To maximize the number of incisions, cuts of both orientations were made along either side of the sagittal suture. However, a number of samples were deemed unusable because the dural tissue had been torn either during the dissection or incising phases.

Microscopy was carried out in the Notre Dame Integrated Imaging Facility, University of Notre Dame, using a Nikon AZ 100 Macro/Zoom Scope with a Nikon DS-L2 camera unit attached to the microscope. To capture potentially time-dependent behavior, images were taken immediately after cutting and five minutes later. The dural incisions were recorded between $1\times$ and $4\times$ magnification. Across three experimental dates, images of 15 dural incisions from 11 subjects (n=5 neonatal, n=6 adult) at two time points were recorded and measured. The incision opening lengths (l) and widths (w) were measured in ImageJ (Rasband 2018) for

all samples, and the normalized opening $(\overline{w}, \text{ width:length})$ was calculated. To ensure consistency in measurements, the width was measured at the midpoint of the cut (at l/2) (Fig. 4). The cut lengths and widths for the 15 dural incisions at T=0 min were averaged according to cut orientation and age group (Table 1).

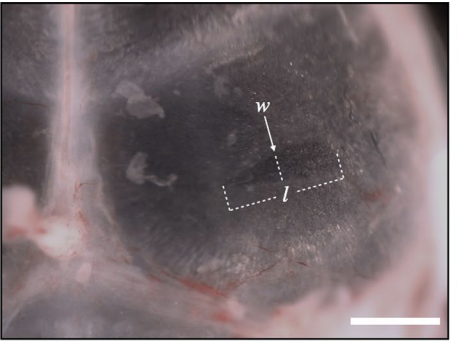
Additional images were taken of a single fully dissected cranium from each age group without the nasal lobe, allowing the dimensions of the skull to be measured and used for estimation of the in silico model's dimensions (Sect. 2.2.3). In ImageJ (Rasband 2018), the boundaries of samples were identified in the lateral, anterior, and posterior views of both the neonatal and adult mice (Fig. 5), and the dimensions were measured and recorded (Table 1). While the dura mater was not visible, the cranium was so thin that it was assumed there was nearly negligible difference between the length, width, and height of the skull and dura.

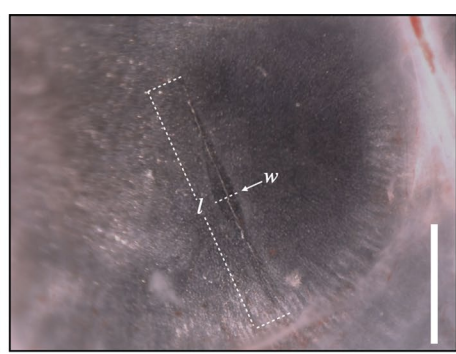
2.2 In silico model of dural prestretch and incisions

2.2.1 Kinematic model of prestretch

Here, we want to generate a model with a realistic geometry and a desired level of isotropic prestretch, λ_p . (As a

Fig. 4 Measurement of incision opening lengths (*l*) and widths (*w*). Widths were measured at the midpoint of the total length. All scale bars indicate 1 mm





transverse

longitudinal



Fig. 5 Measurement of neonatal (left) and adult (right) mice skull/dura mater dimensions. All scale bars indicate 1 mm

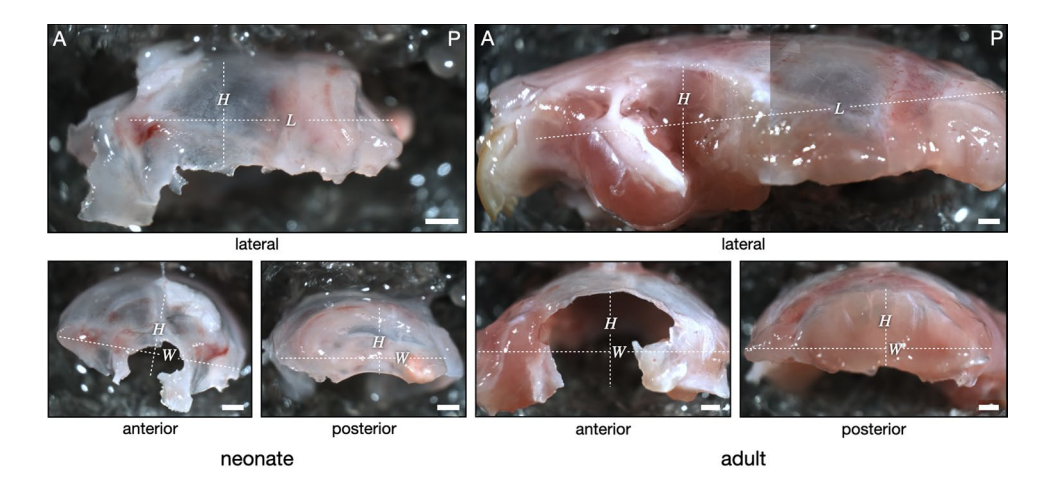


Table 1 Ex vivo cranial dimensions and dural incision opening length and width measurements at T=0 min

Age group	n	<i>L</i> [mm]	W [mm]	H [mm]	Cut orientation	# cuts	<i>l</i> [mm]	w [mm]
Neonate	5	8.67	8.56	2.88	Transverse	2	1.07 ± 0.28	0.18 ± 0.09
					Longitudinal	5	1.83 ± 0.47	0.18 ± 0.10
Adult	6	18.63	13.01	4.59	Transverse	4	1.76 ± 0.41	0.41 ± 0.15
					Longitudinal	4	2.58 ± 0.31	0.23 ± 0.09

note, here we use two-dimensional terminology referring to the dura mater, which can be approximated as a twodimensional membrane. Thus, isotropic refers to a material with identical properties throughout the plane, while it may have different properties in the thickness direction; in a three-dimensional setting, this would be considered transversely isotropic. Similarly, anisotropic is used to refer to materials with different properties in different directions within the plane.) We begin by adopting the framework of finite growth (Rodriguez et al. 1994), where the total deformation is multiplicatively decomposed into a stress-free deformation followed by an elastic deformation. In this case, in short, we begin with a stress-free body and apply a stress-free deformation and two elastic deformations, the first of which represents the prestretching, and the second of which represents the opening of the cut.

We begin with a fictitious stress-free body \mathfrak{B}_0 (Fig. 6) and first apply a stress-free deformation (F^0) that creates a smaller, thicker tissue \mathfrak{B}_1 . This configuration is reminiscent of the ex vivo state of the dura mater, in which the excised tissue, free of bony attachments, retracts to a smaller, relaxed sample. This is then followed by an elastic deformation representing prestretch (F^p) that returns it to the original geometry via elastic stretch. The total deformation gradient between the fictitious initial configuration and the in vivo stretched configuration is equal to the identity (I). It can be decomposed into the two deformations described above as $F = I = F^p \cdot F^0$, such that the induced prestretch can be found from the stress-free deformation F^0 as

$$\mathbf{F}^{p} = (\mathbf{F}^{0})^{-1} \,. \tag{1}$$

Here, we investigate the effects of isotropic area prestretch λ_p (Rausch and Kuhl 2013), such that the prestretch deformation has the form

$$F^{p} = \lambda_{p}[I - \mathbf{n}_{0} \otimes \mathbf{n}_{0}] + \frac{1}{\lambda_{p}^{2}} \mathbf{n}_{0} \otimes \mathbf{n}_{0}$$
(2)

where n_0 is the reference unit vector normal to the surface at each point.

From the prestretched configuration, a second elastic deformation \mathbf{F}^{cut} results from the cut. The total elastic deformation, then, is the composition of the prestretch and cut deformations, $\mathbf{F}^{\text{e}} = \mathbf{F}^{\text{cut}} \cdot \mathbf{F}^{\text{p}}$. Alternately, it can more easily be found from \mathbf{F} , the total deformation gradient from Abaqus, as

$$\mathbf{F}^{e} = \mathbf{F} \cdot (\mathbf{F}^{0})^{-1} = \mathbf{F} \cdot \mathbf{F}^{p} = \mathbf{F} \cdot \left[\lambda_{p} [\mathbf{I} - \mathbf{n}_{0} \otimes \mathbf{n}_{0}] + \frac{1}{\lambda_{p}^{2}} \mathbf{n}_{0} \otimes \mathbf{n}_{0} \right].$$
(3)

Again adopting from the framework of finite growth, the stress is a function only of this elastic deformation (Rodriguez et al. 1994).

As here, we are only investigating time-independent elastic deformation, we efficiently simulate multiple values of prestretch by changing the prestretch linearly in simulation "time",



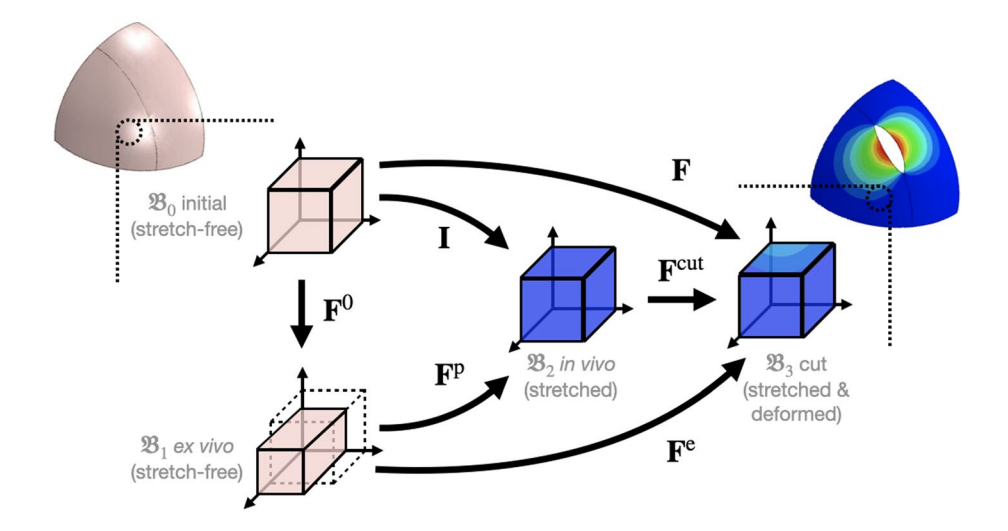


Fig. 6 Kinematics of finite stretching and post-dural incision deformation of the mouse cranial dura mater. The 1/8 ellipsoid shapes are an idealized geometry which represent the neonate and adult dura. The initial stress-free model (top left) is a fictitious configuration only known to Abaqus. The in vivo stretched configuration is created through an inelastic deformation which creates a stress-free

thicker, smaller tissue (F^0) and an elastic deformation that stretched it to achieve the same geometry under prestretch (F^p) . A second elastic deformation represents the cutting experiment (F^{cut}) . The total elastic deformation is determined from $F^e = F \cdot (F^0)^{-1}$, where F is the total deformation recorded by Abaqus

$$\lambda_{p,i} = 1.0 + (\lambda_{p,f} - 1.0) \frac{t_i}{t_f},$$
(4)

where $\lambda_{\mathrm{p},i}$ is the prestretch at time t_i and $\lambda_{\mathrm{p},f}$ is the prestretch at the end of the simulation, t_{f} . Likewise, we measure the cut opening at each timepoint to obtain a relationship between prestretch and cut opening.

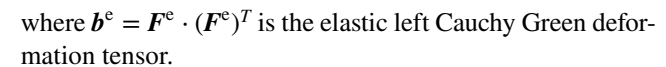
2.2.2 Constitutive model and governing equations

Several uniaxial (Maikos et al. 2008; Noort et al. 1981; Wolfinbarger et al. 1994; Zwirner et al. 2019) and biaxial (Bylski et al. 1986; Kriewall et al. 1983) loading studies, across multiple mammals (human, rat, and pig), have shown that cranial dura mater deforms non-linearly, requiring that a hyperelastic constitutive model must be used to mimic the tissue's stress–strain behavior. Here, we model the dura mater as a slightly compressible neo-Hookean material, with the strain energy density function given by:

$$\Psi(\mathbf{F}^{e}) = \frac{\mu}{2} \left[\text{tr}(\mathbf{C}^{e}) - 3 - 2 \ln (J^{e}) \right] + \frac{\lambda}{2} \ln^{2} (J^{e}),$$
 (5)

where $C^{\rm e} = (F^{\rm e})^T \cdot F^{\rm e}$ is the elastic right Cauchy Green deformation tensor, $J^{\rm e}$ is the determinant of the elastic deformation gradient, and μ and λ denote shear modulus and Lamé constant, respectively. The Cauchy stress is then given by

$$\sigma = \frac{1}{J^{e}} [\mu b^{e} + (\lambda \ln(J^{e}) - \mu) I], \qquad (6)$$



We used stress-stretch data from rat cranial dura mater under uniaxial tension (Maikos et al. 2008) to calibrate our constitutive model, as experimental data on mouse dura was not available. Specifically, we found the shear modulus by fitting the model to data from 0 to 8% strain, while choosing $\lambda = 100\mu$ to ensure low compressibility. This regime was chosen because we are primarily interested in deformation under initial stretching, resulting in a value of 1.127 MPa.

Finally, with the model quasi-statically deforming and no active body forces applied, Cauchy's first equation of motion is solved simply by

$$\nabla \cdot \boldsymbol{\sigma} = \boldsymbol{0} \,. \tag{7}$$

The mathematical and constitutive models were implemented on the constrained domain within Abaqus/Standard by writing a user-defined material (UMAT) subroutine (Holland 2018).

2.2.3 Model geometry, mesh, and boundary conditions

An ellipsoid was chosen as a reasonable representation of the dura, with the dimensions of the ellipsoid determined from the measured skull dimensions (Table 1). Assuming symmetry in the axial, coronal, and sagittal planes, the geometry was further simplified to a one-eighth ellipsoid (Fig. 7). The major axis was defined as half of the measured length, based on existing experimental measurements of ICR mice, which reported that the parietal, interparietal,



and occipital lobes made up roughly half of the total length, excluding the nasal lobe (Kawakami and Yamamura 2008). The minor axes of the ellipsoid were set to half of the measured width (Table 2).

The thickness of the dura mater could not be extracted from the images. Instead, mouse dural thickness was estimated by using a proportional relationship of rat dura:skull thickness to mouse dura:skull thickness, which was thought to be appropriate because of the anatomical and phylogenetic similarities between mice and rats (Constantinescu 2018; Frohlich 2020). Another proportional relationship was used to estimate newborn dural thickness based on the ratios of the adult and neonatal dimensions (Table 2). Homogeneous thickness was assumed throughout each model. While human dural thickness has been shown to vary locally (Fam et al. 2018; Kuchiwaki et al. 1997), heterogeneous thickness

was expected to have negligible effects because the thickness of both age groups was on the order of 0.01 mm.

Four models were created: neonatal and adult dura mater, with both transverse and longitudinal incisions (Fig. 7). Each model consisted of two parts: a deformable dura mater, and a rigid shell representing the brain (below the dura mater, not visible in Fig. 7). The rigid shell was fixed in place, and a surface-to-surface interaction between the two ensured that the dura mater would maintain its curvature throughout deformation. The dura mater was assigned roller conditions along the axial, coronal, and sagittal planes of symmetry.

To represent the incisions, the models were partitioned in either the coronal plane for the transverse incision, or the sagittal plane for the longitudinal incision. In both cases, the cut was located at the middle of the axis (*a*/2 and *b*/2, respectively) to match the experimental incisions. Tie constraints

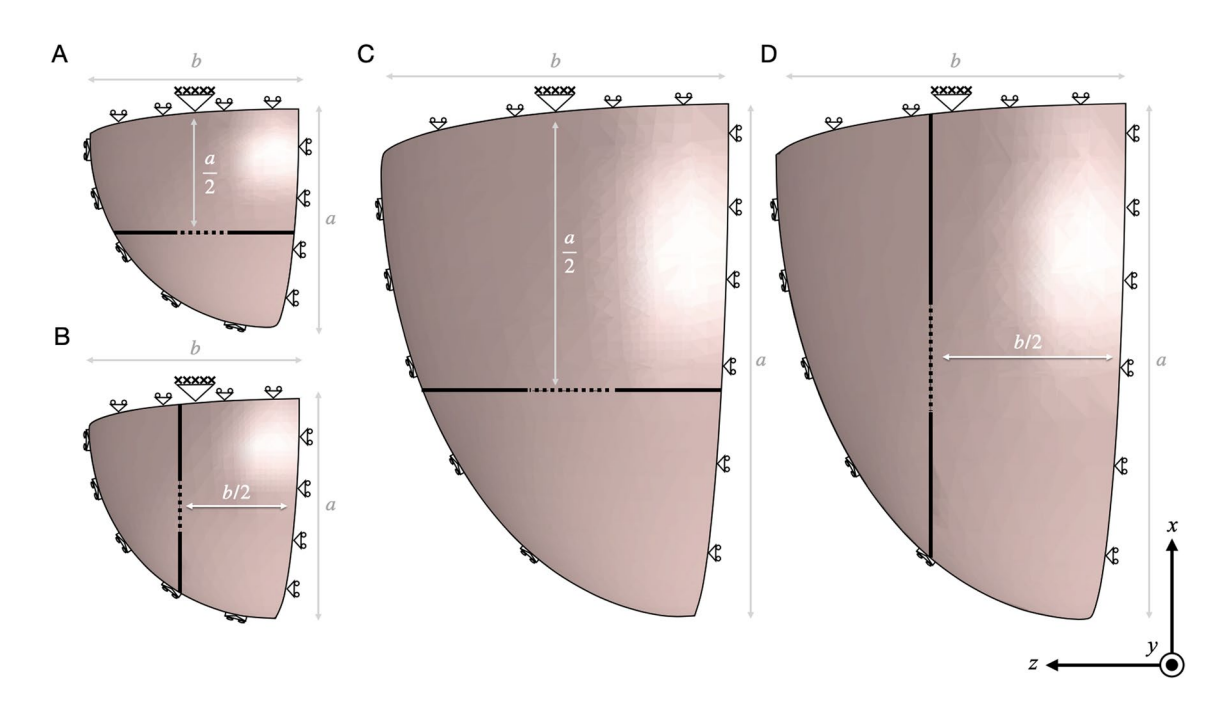


Fig. 7 In silico models of neonatal and adult mouse cranial dura mater. Symmetry was used to simplify the models into one-eighth ellipsoids. The major axis (a) and minor axis (b) of the neonatal (A and B) and adult (C and D) skulls were taken from experimental measurements. Roller boundary conditions were applied on all symmetric planes of the one-eighth ellipsoid. The deforming dura mater has a surface-to-surface interaction with a fixed rigid shell (not visi-

ble here), ensuring there is no change in curvature throughout stretching. Transverse (**A** and **C**) and longitudinal (**B** and **D**) cuts were simulated by partitioning the models along the appropriate plane. The split parts were joined with tie constraints (solid black line) along most of the partition, while the initial cut lengths (l_0) were made in the middle of the models and left unconstrained (dotted black line)

Table 2 In silico model dimensions, thickness, initial cut lengths, and total number of elements within each in silico model

Age group	Major axis (a) [mm]	Minor axis (b) [mm]	t [mm]	Cut orientation	<i>l</i> ₀ [mm]	C3D4H	R3D3	R3D4
Neonate	4.337	4.278	0.008	Transverse Longitudinal	1.067 1.829	86980 80581	202	7407
Adult	9.315	6.506	0.014	Transverse Longitudinal	1.764	220028 254019	740	22133



bonded the two parts together, except for an unconstrained region the length of the cut (Table 2), which was based on the length of the ex vivo incisions (Table 1).

The dura mater was discretized with four-noded linear tetrahedral hybrid elements with linear pressure variation (C3D4H). Linear triangular (R3D3) and quadrilateral (R3D4) rigid elements were used for the rigid shell (Table 2).

2.2.4 Statistics

The experimental normalized incision openings (width:length), $\overline{w}_{\rm E}$, were calculated from the measurements taken at T=0 min and are presented as mean \pm standard deviation. From the the simulated data, $\overline{w}_{\rm S}$ was calculated at each increment of the simulation, resulting in a relationship between the prestretch $\lambda_{\rm p}$ and the normalized opening. By comparing each value of $\overline{w}_{\rm E}$ with the values of $\overline{w}_{\rm S}$ found at a given level of prestretch, we estimated the prestretch in the experimentally tested tissue (Figs. 8, 9). Specifically, the in-plane prestretches were estimated from the intersection of the in silico opening ratio–stretch curve and the average of the ex vivo opening ratios. These estimated prestretch values were then averaged for each group (age × cut orientation) (Table 3, Fig. 9), and the standard deviation was calculated.

A series of Mann–Whitney U tests were performed to determine if there were significant differences in \overline{w}_E and λ_p between the cut orientations and age groups. Differences

were considered statistically significant when p < 0.05 and are indicated with * in Fig. 9.

3 Results and discussion

3.1 Estimation of dural prestretch

The first objective of this study was to estimate the prestretch present in mouse cranial dura mater. By comparing our experimental incision openings with predicted values from simulations (Fig. 8), we estimate the isotropic in-plane prestretches for both age groups and incision orientations (Table 3, Fig. 9).

By multiplying the prestretches in each direction together, we can estimate the in-plane area prestrain to be 11% and 14% in neonatal and adult mice, respectively. In the rat dura mater, this is well outside of the linear toe regime, suggesting that the dura mater is likely notably stiffer in its

Table 3 Experimental normalized opening $\overline{w}_{\rm E}$ and estimated dural prestretch $\lambda_{\rm p}$

Age group	Cut orientation	$\overline{w}_{ m E}$	$\lambda_{ m p}$
Neonate	Transverse	0.167 ± 0.039	1.067 ± 0.018
	Longitudinal	0.095 ± 0.043	1.040 ± 0.020
Adult	Transverse	0.230 ± 0.073	1.098 ± 0.040
	Longitudinal	0.092 ± 0.046	1.035 ± 0.019

Fig. 8 In silico curves for estimation of prestretch. Mean (dotted lines) \pm standard deviation (light blue shading) of experimental normalized opening $\overline{w}_{\rm E}$ are compared against the relationship between prestretch $\lambda_{\rm p}$ and in silico normalized opening $\overline{w}_{\rm S}$ (solid black line) for neonatal (A, B) and adult (C, D) mice with transverse (A, C) and longitudinal (B, D) dural incisions. The dark blue shading indicates the confidence range of the estimated pre-stretch

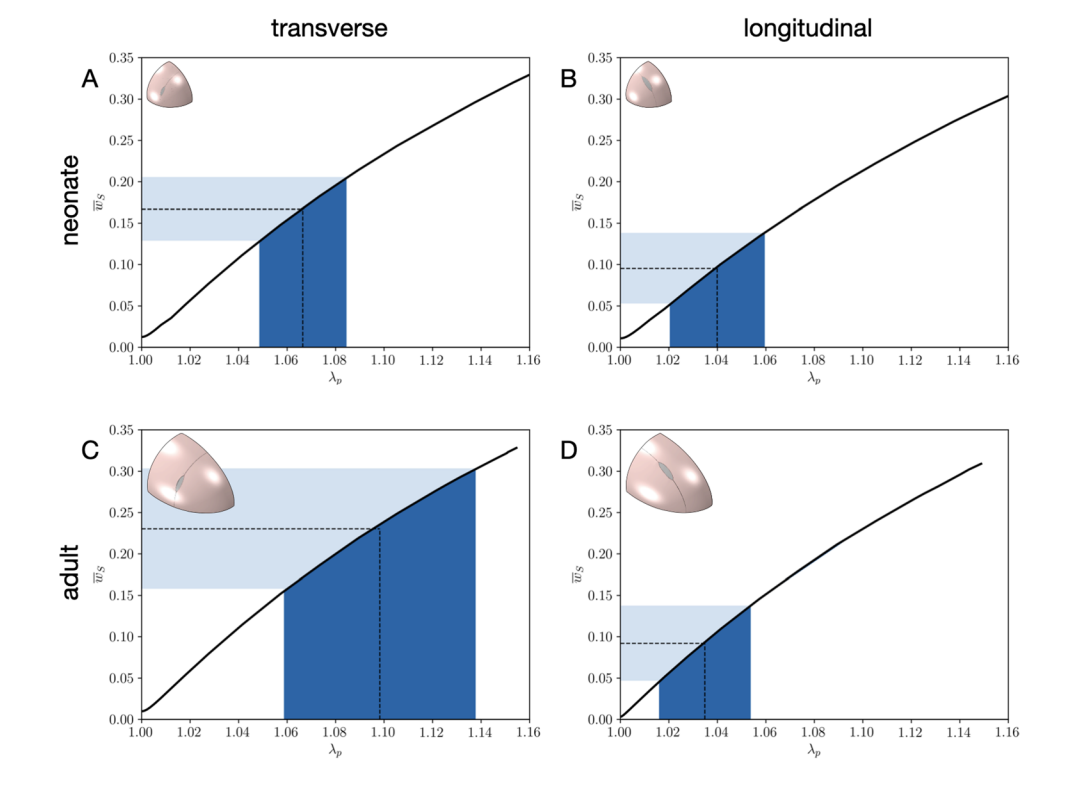
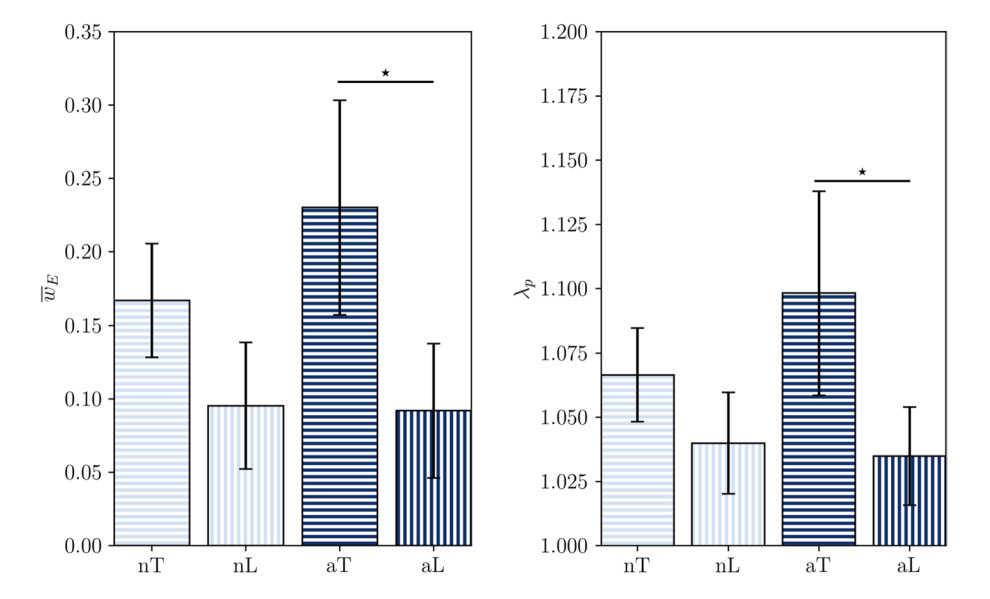




Fig. 9 Bar plot of average (\pm standard deviation) normalized opening values and estimated prestretch for each group. * indicates statistical significance, p < 0.05



prestretched in vivo state (Maikos et al. 2008). This could be advantageous in limiting the motion of the brain. For example, the falx cerebri, a fold of the dura mater that separates the hemispheres of the brain and is thought to constrain the motion of the brain, is significantly stiffer than the surrounding tissue (Bradshaw et al. 2001).

3.2 Effect of curvature on incision opening

Along with estimating dural prestretch, we also aimed to improve upon a previous study (Henderson et al. 2005) by developing an in silico model that better captures the dura's in situ tissue size, geometry, and curvature. Their model considered the dura mater as a two-dimensional rectangle, while our proposed model is a three-dimensional 1/8 ellipsoid. The previous study argued that a flat model is appropriate because the incisions are small relative to the curvature of the dura. To assess the validity of this claim, we investigated the role of curvature on tissue retraction. Here, we changed the curvature of the dura model simulations by scaling the adult mouse model up and down while maintaining the aspect ratio and average element size. The relative cut size was also held constant at $l_0 = b/4$ and a/4 for the transverse and longitudinal cuts, respectively. The opening ratio was recorded for models of increasing axes lengths, which results in decreasing curvature (Fig. 10). For comparison, we include the results from a prior study (Henderson et al. 2005) that used a flat domain (i.e., a domain with zero curvature).

When varying the major and minor axes of our ellipsoid, we observed that the normalized opening decreases only slightly with increasing curvature in both cut orientations (Fig. 10). However, when including the results from a previous study in a flat (i.e., zero curvature) domain (Henderson et al. 2005), we see a dramatic increase. This suggests that

a flat model may greatly overestimate the incision opening, and thus underestimate prestretch, and that three-dimensional models are necessary for more accurate estimations.

3.3 Effect of initial incision length on incision opening

In order to meaningfully relate our results with prior findings in the literature, we used the normalized incision openings to estimate prestretch. \overline{w} had previously been used in the literature (Henderson et al. 2005), as a dimensionless parameter that allows for comparison between cuts for different sizes. However, we sought to judge the validity of this measurement by comparing cuts across varying initial lengths. Using the adult mouse model, we simulated transverse and longitudinal incisions ranging from 0.407 to 3.253 mm (from $l_0 = b/16$ to b/2) and 0.582 to 4.658 mm (from $l_0 = a/16$ to a/2), respectively. The resulting normalized openings were compared between different-sized cuts (Fig. 11).

Our results (Fig. 11) generally support the previous assumption, showing that when the initial cut size is small, it does not meaningfully impact the incision opening. However, as initial incision size becomes larger (e.g., $l_0 = a/2$ or b/2), the normalized opening is noticeably lower than in smaller incisions. In the case of our models, our initial incision sizes are taken from experimental measurements, and are fairly large relative to the model geometry $(a/4 < l_0 < a/2 \text{ or } b/4 < l_0 < b/2 \text{ for transverse}$ and longitudinal cuts, respectively). The previous study reports their incision sizes but not the size of the rat crania, which makes it impossible to determine if their incisions could be considered 'small' or not. Based on these results, the normalized incision opening is a decent, but not perfect, metric to



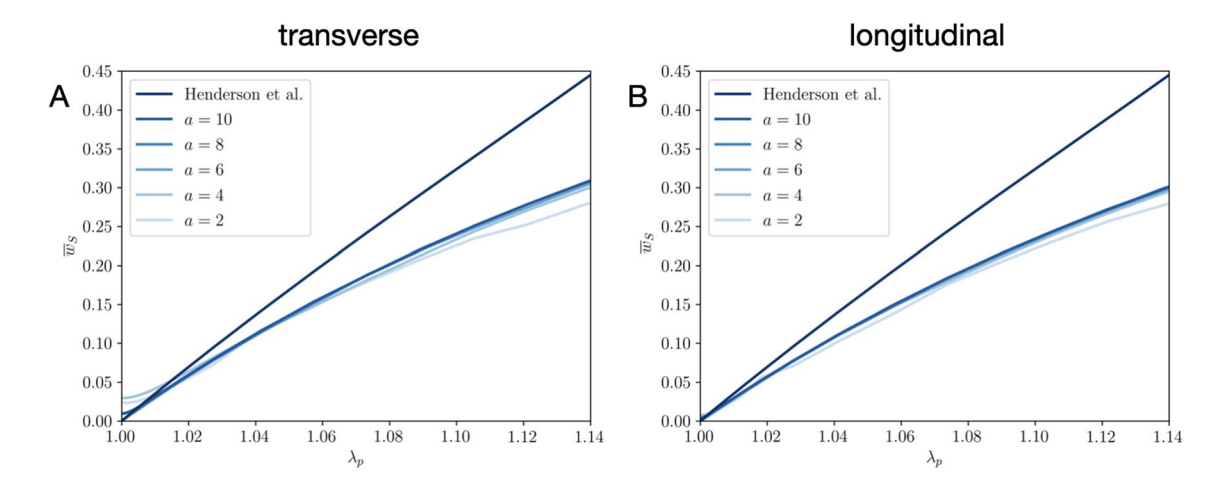


Fig. 10 Effect of model curvature on incision opening. Normalized opening \overline{w}_S vs. prestretch λ_p for transverse (**A**) and longitudinal (**B**) incisions in models with varying curvature. Results from a previ-

ous study on a flat (i.e., zero curvature) domain are also shown (dark blue); the equation is taken from the special case of isotropic area stretch (Henderson et al. 2005)

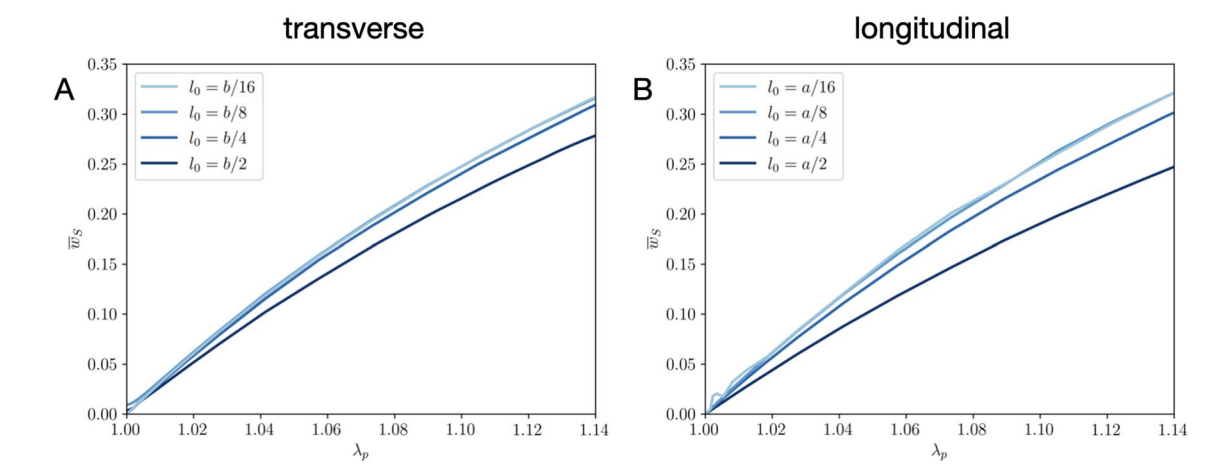


Fig. 11 Effect of incision length on normalized opening. \overline{w}_S vs. λ_p for a range of initial cut lengths for both transverse (A) and longitudinal (B) cuts

evaluate opening widths across cuts of different sizes within this range.

3.4 Analysis of direction dependency

The second objective of this study was to determine the directional dependency in dura mater prestretch. When comparing the estimated prestretch from the transverse and longitudinal cut openings in both age groups, the adult is found to have significantly higher prestretch in one direction, while there is no significant difference between the two directions in the neonate. The "in-plane" prestretch implemented here is equibiaxial and does not directly represent different values of prestretch along the transverse and longitudinal axes. However, higher in-plane stretches associated with transverse incisions in the adult suggest that the

anterior–posterior, or longitudinal, stretch is larger than the medial–lateral or transverse stretching. This is also visible qualitatively, as the transverse cuts open noticeably more than the longitudinal cuts in both the adult and neonatal cranial dura. This is in agreement with previous results (Henderson et al. 2005), which also found significantly larger residual strains in the longitudinal (6.11 \pm 3.62%) than transverse (3.82 \pm 2.64%) directions.

We note that these results could also, but do not necessarily, suggest material anisotropy of the dura mater. Several investigations including scanning electron microscopic imagery (McGarvey et al. 1984; Patin et al. 1993; Wolfinbarger et al. 1994) and small-angle light scattering (Jimenez et al. 1998) have found that human dura mater is globally isotropic, without any predominant fiber direction. However, a comparison of humans and rats has shown that rat dura



mater has noticeably longer and frequent longitudinal fibers, with small and less-frequent transverse fibers (Maikos et al. 2008). Variation across mammals is common for biological tissues. Similarly, lumbar dura mater is known to be structurally anisotropic in rats, canines, and humans (Maikos et al. 2008; Patin et al. 1993). Microscopic imaging would be needed to distinguish material vs. loading anisotropy in mouse cranial dura.

3.5 Analysis of age dependency

The third objective was to examine the age dependency of the prestretch by comparing neonatal and adult values. Although only two time points were obtained, our results suggest that prestretch is not strongly age dependent, as no significant differences were found in comparisons between the neonate and adult mice (Fig. 9). A similar study in rats (Henderson et al. 2005) similarly observed no significant relationship between age and prestretch. However, our data suggests there is a relationship between age and direction dependence, as the neonatal dural prestretch was slighty more isotropic than the adult. We hypothesize that cranial shape may play a role in defining dural prestretch, particularly that the more spherical neonatal skull contributes to uniform strain. Our length and width measurements clearly show that the neonatal neurocranium is nearly spherical and is stretched more isotropically than the hemi-ellipse mature cranium (Table 1, Fig. 5). Interestingly, humans, who also have more rounded heads, are consistently reported to have mechanically and materially isotropic dura mater (Jimenez et al. 1998; McGarvey et al. 1984; Patin et al. 1993; Wolfinbarger et al. 1994).

Another possible factor is the direction dependence of skull growth; higher longitudinal prestretch in immature rats has been hypothesized to be related to the growth of the cranial vault, preferentially in the longitudinal direction (Henderson et al. 2005). Rats and mice have been shown to follow nearly identical developmental timelines (Clancy et al. 2007; Workman et al. 2013) thus we can speculate increased longitudinal stretching would be present within the mouse. However, because the mouse crania is more stout and much smaller, the directional differences may be less pronounced.

3.6 Estimation of dural growth

By combining our estimations of pre-stretch with our calculations of areal growth of the dura mater, we can estimate the relative contributions of growth (i.e., the addition of mass) and stretch between 4 and 12 weeks (Fig. 1). From our in vivo imaging data, the dura mater was calculated to grow in area by approximately 7%, on average, during that time (Fig. 12). (Note that two additional imaging timepoints

were also completed, at 16 and 20 weeks, and are available with the rest of the data from this paper; they are not included in our analyzes in order to make the best comparison with our experimental data.) Area prestretch increases only slightly from the neonate to the adult (Fig. 1 4d-12w), 11–14%. Taken together, this suggests that little of the area expansion is due to stretch, and that the dura mater grows in area by nearly 7% during this period.

While a rigorous analysis of this is out of scope of the current work because of the difficulty of imaging neonatal mice, these findings are likely related. It is understood that the dura mater contributes to cranial suture fusion by releasing osteogenic growth factors that induce cellular proliferation, mineralization, and differentiation in response to increased pressure from the growing brain (Fabris et al. 2019; Gagan et al. 2007; Jaslow 1990; Ogle et al. 2004). Previous work (Fong et al. 2003) has shown that immature dural cells proliferate markedly more than their mature counterparts at high levels of strain ($\sim 10\%$). This is close to our estimated strain, suggesting that the dura is stretched in vivo to lead to optimal conditions for growth and suture fusion. These results raise important questions about the interplay between mechanical loading and dural growth, particularly in the case of cranial growth pathologies.

3.7 Relaxation of dural incisions

Because we obtained images of the experimental tissue at T=0 to T=5 min after incision, we were able to investigated the time-dependent behavior of the dura mater. We quantified the tissue relaxation by calculating the percent change in the normalized incision opening as the tissue relaxed from T=0 to T=5 min. The percent change was

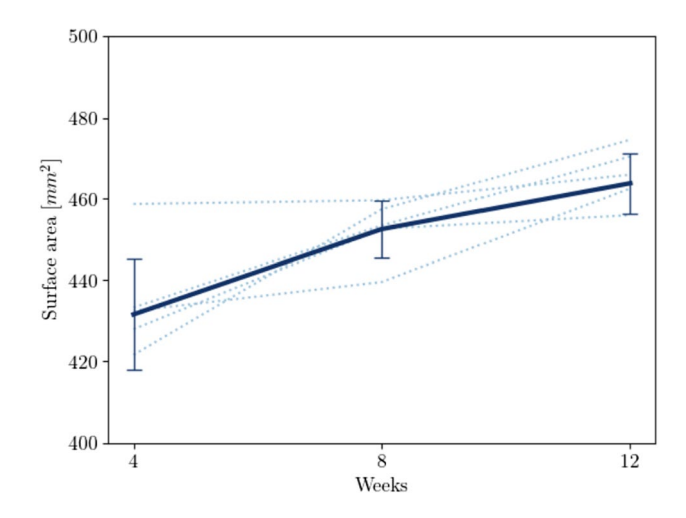


Fig. 12 Brain/dural surface area during development in mice. Data from five individuals are shown in light blue, along with average and standard deviation in dark blue



calculated for each cut, and then averaged within groups (Table 4).

In general, most incisions saw an increase in size. This time-dependent behavior suggests that the mouse dura mater is viscoelastic, because the initial elastic retraction of the dura after incision is followed by a creep unloading response. However, the high standard deviations, particularly in the transverse incisions, indicate the limitations of our small sample size. A few cuts actually appeared to decrease in cut area, mostly slight (~ 2%) but in one case fairly significant (14% in a neonatal transverse cut). We believe that these samples were outliers, perhaps due to how the cranium was held during and after the incision. Specifically, the cranium was generally held with tweezers throughout the incision, but at times the skull had to be secured by pressing down on it from the superior position. This could have slightly stretched the skull, leading to the appearance of cut closing as the skull was released. We note that previous results in rats have shown greater consistency (Henderson et al. 2005), potentially due to their larger size and the relative ease of experiments.

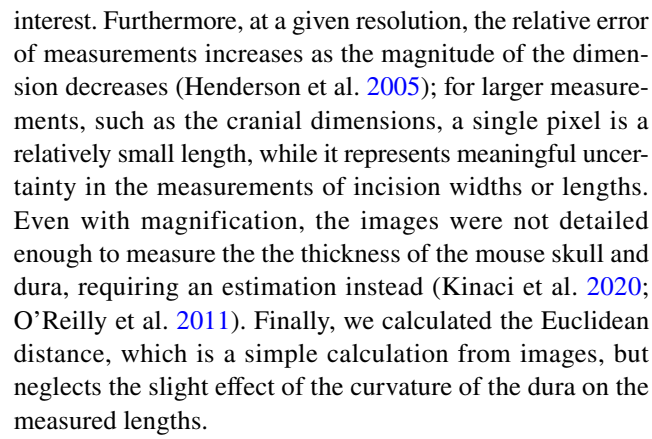
4 Limitations

While this study is the first to develop a three-dimensional model of the dura mater in order to estimate in vivo prestretch, significant future work remains to address its limitations and fully resolve the outstanding questions. First of all, our investigation is limited by a small experimental size (n = 5 neonate, n = 6 adult). The small size of the dural tissue made consistent cutting very difficult, further exacerbating the small sample size. Most notably, the in-plane prestretch associated with the transverse neonatal incisions was estimated based on the normalized opening from just two subjects, which differed appreciably. Measurements from more subjects would give us an idea of the true variability among individuals.

Secondly, the precision of our measurements was limited. One of the main limiting factors was the image resolution, for instance affecting the manual estimation of points of

Table 4 Normalized incision openings before and after relaxation, along with calculated change between T=0 and T=5 min

Age group	Cut orienta- tion	$\overline{w}_{\mathrm{E}}$	$\delta_{\overline{w}}$ [%]	
		$T = 0 \min$	$T = 5 \min$	
Neonate	Transverse	0.167 ± 0.039	0.171 ± 0.073	0.17 ± 20.72
	Longitudinal	0.095 ± 0.043	0.106 ± 0.045	11.82 ± 5.89
Adult	Transverse	0.230 ± 0.073	0.244 ± 0.072	6.62 ± 12.85
	Longitudinal	0.092 ± 0.046	0.094 ± 0.043	3.95 ± 4.83



Furthermore, the cutting method has its limitations. It primarily approximates only stretch perpendicular to the cut. These cuts are also generally thought to capture only the environment local to the cut, although given the relatively large size of our incisions (12 – 21% of the relevant dimension of the skull), it could be argued that they capture more global behavior. Furthermore, there are inherent limitations to estimating in vivo prestretch from ex vivo data, even though the tissue was hydrated with PBS, its in situ connection to the skull was maintained, and the testing was performed within a few hours of sacrifice. Additionally, the thickness of the scalpel blade, while small (0.4 mm), could make it hard to determine the cause of very small opening widths, and potentially lead to overestimation of prestretch.

Additionally, no experimental stress-strain data were available for the ICR mouse dura; instead, our constitutive models were calibrated on experimental data from mature rats, which are likely even less accurate for neonatal mice. Likewise, the neo-Hookean constitutive model does not fully capture the nonlinear behavior of the dura mater. To address this, we calibrated the shear modulus only to the relevant regime (ε < 8%). This was an acceptable limitation for this study because of its focus on the effects of size and curvature, but future in silico works should consider modeling the tissue with other hyperelastic models, such as an Ogden model with N = 3 (Maikos et al. 2008; Pierrat et al. 2020) or other higher order alternatives (e.g., Skalak, Tozeren, Zarda, and Chien) (Bylski et al. 1986; Kriewall et al. 1983). It could also be important to incorporate viscoelastic behavior directly, as relaxation after cutting has been recorded in human (Melvin et al. 1970), rat (Henderson et al. 2005; Maikos et al. 2008; Shulyakov et al. 2011), and now mouse dura mater.

Moreover, while our three-dimensional model represents a significant step forward in capturing the effect of curvature on dural prestretch, the one-eighth ellipsoid used does not capture the full complexity of the dura's initial shape. For example, the minor axes of the ellipsoid were set equal to each other because of limitations in Abaqus, which resulted in the measured height being neglected. Other irregularities



and imperfections were also lost when simplifying to an ellipsoid. In addition to the finite element method used here, other approaches such as isogeometric analysis could offer more representative models of the in vivo tissue (Laurence et al. 2022).

Finally, the general applicability of our prestretch findings are limited by the failure to consider heterogeneous strain. Concentrations have been previously reported along the suture sites (Herring and Teng 2000; Curtis et al. 2013), indicating that the developing dura mater is likely non-uniformly prestretched. Future models could aim to simulate the geometric and mechanical influence of sutures by modeling anisotropic, heterogeneous residual strain. Characterizing prestretch variation could be accomplished through the current method by making isolated incisions within and far from the suture site. While difficult to target areas in small mammals, this would be possible in larger mammals, while additionally offering a more apt comparison to human dura.

5 Conclusions

In this study, we created accurately sized three-dimensional in silico models of neonatal and adult mouse cranial dura mater with longitudinal and transverse incisions. Alongside experimental measurements of incision opening ratios, we estimated the magnitude of in-plane prestretch. We found inplane prestretches ranging from 3 to 10%, and corresponding area stretches of 11–14%, with slightly higher values in adult mice. Significantly larger in-plane prestretch perpendicular to the transverse cuts indicated anisotropy in the adult mice, consistent with previous findings in rats (Henderson et al. 2005). Future work could continue to improve on this study by experimentally calibrating a higher-order constitutive model, including viscoelastic behavior, and implementing anisotropic and/or heterogenous prestretch. Additionally, while our study has focused solely on the dura along the curved endocranial surface of the vault, the basicranial surface, which is morphologically more complex with convex and concave surfaces, could be a profitable target for future research. Our results highlight the importance of in situ experimental testing and accurate in silico modeling when estimating the in vivo mechanical properties of cranial dura mater. This work is essential because advanced mechanical characterization may provide insight into how common cranial malformations arise and could guide clinicians toward more appropriate natural and synthetic grafts for dural repair.

Acknowledgements This project was supported by NSF Grant Nos. IIS-1850102 (to M. A. Holland) and BCS-1848884 (to M. J. Ravosa), the Indiana Clinical and Translational Sciences Institute (to M. A. Holland, M. J. Ravosa, and C. J. Goergen; funded, in part, by grant no. UL1TR002529 from the NIH National Center for Advancing

Translational Sciences, Clinical and Translational Sciences Award), the NIH National Heart, Lung, and Blood Institute (F30-HL145980 to F. W. Damen), and the Leslie A. Geddes Endowment at Purdue University (to C. J. Goergen). The content is solely the responsibility of the authors and does not necessarily represent the official views of the NIH or NSF.

Data availablity Original data (images, measurements, etc.) and scripts to run all simulations and analysis are available at https://github.com/mholla/BMMB24.

Declarations

Conflict of interest The authors declare that they have no conflict of interest.

References

- Abuzayed B, Kafadar AM, Oğuzoğlu A, Canbaz B, Kaynar MY (2009) Duraplasty using autologous fascia lata reenforced by on-site pedicled muscle flap: technical note. J Craniofac Surg 20(2):435–438. https://doi.org/10.1097/SCS.0b013e31819b968f
- Aydin S, Kucukyuruk B, Abuzayed B, Aydin S, Sanus GZ (2011) Cranioplasty: review of materials and techniques. J Neurosci Rural Pract 02(2):162–167. https://doi.org/10.4103/0976-3147. 83584
- Aydin HE, Kizmazoglu C, Kaya I, Husemoglu B, Sozer G, Havitcioglu H, Arslantas A (2019) Biomechanical properties of the cranial dura mater with puncture defects: an in vitro study. J Korean Neurosurg Soc 62(4):382–388. https://doi.org/10.3340/ jkns.2018.0130
- Becker SS, Jackler RK, Pitts LH (2003) Cerebrospinal fluid leak after acoustic neuroma surgery: a comparison of the translabyrinthine, middle fossa, and retrosigmoid approaches. Otol Neurotol Off Publ Am Otol Soc Am Neurotol Soc Eur Acad Otol Neurotol 24(1):107–112. https://doi.org/10.1097/00129492-20030 1000-00021
- Borghi A, Rodriguez-Florez N, Rodgers W, James G, Hayward R, Dunaway D, Jeelani O, Schievano S (2018) Spring assisted cranioplasty: a patient specific computational model. Med Eng Phys 53:58–65. https://doi.org/10.1016/j.medengphy.2018.01. 001
- Bradshaw DRS, Ivarsson J, Morfey CL, Viano DC (2001) Simulation of acute subdural hematoma and diffuse axonal injury in coronal head impact. J Biomech 34(1):85–94. https://doi.org/10.1016/s0021-9290(00)00135-4
- Buganza Tepole A, Gart M, Gosain AK, Kuhl E (2014) Characterization of living skin using multi-view stereo and isogeometric analysis. Acta Biomater 10(11):4822–4831. https://doi.org/10.1016/j.actbio.2014.06.037
- Buganza Tepole A, Gart M, Purnell CA, Gosain AK, Kuhl E (2015) Multi-view stereo analysis reveals anisotropy of prestrain, deformation, and growth in living skin. Biomech Model Mechanobiol 14(5):1007–1019. https://doi.org/10.1007/s10237-015-0650-8
- Bylski DI, Kriewall TJ, Akkas N, Melvin JW (1986) Mechanical behavior of fetal dura mater under large deformation biaxial tension. J Biomech 19(1):19–26. https://doi.org/10.1016/0021-9290(86)90105-3
- Chaudhry HR, Bukiet B, Findley T, Ritter AB (1998) Evaluation of residual stress in rabbit skin and the relevant material constants. J Theor Biol 192(2):191–195. https://doi.org/10.1006/jtbi.1997.0616



- Clancy B, Kersh B, Hyde J, Darlington RB, Anand KJS, Finlay BL (2007) Web-based method for translating neurodevelopment from laboratory species to humans. Neuroinformatics 5(1):79–94. https://doi.org/10.1385/NI:5:1:79
- Constantinescu GM (2018) Comparative anatomy of the mouse and the rat: a color atlas and text. CRC Press, Taylor & Francis Group. 262 pp. ISBN: 9781138624030
- Curtis N, Jones MEH, Evans SE, O'Higgins P, Fagan MJ (2013) Cranial sutures work collectively to distribute strain throughout the reptile skull. J R Soc Interface 10(86):20130442. https://doi.org/10.1098/rsif.2013.0442
- Fabris G, Suar ZM, Kurt M (2019) Micromechanical heterogeneity of the rat pia-arachnoid complex. Acta Biomater 100:29–37. https:// doi.org/10.1016/j.actbio.2019.09.044
- Fam MD, Potash A, Potash M, Robinson R, Karnell L, O'Brien E, Greenlee JDW (2018) Skull base dural thickness and relationship to demographic features: a postmortem study and literature review. J Neurol Surg Part B Skull Base 79(6):614–620. https://doi.org/10.1055/s-0038-1651501
- Fong KD, Warren SM, Loboa EG, Henderson JH, Fang TD, Cowan CM, Carter DR, Longaker MT (2003) Mechanical strain affects dura mater biological processes: implications for immature calvarial healing. Plastic Reconstruct Surg 112(5):1312–1327. https://doi.org/10.1097/01.PRS.0000079860.14734.D6
- Frohlich J (2020) Rats and mice. Ferrets Rabbits Rodents. https://doi. org/10.1016/B978-0-323-48435-0.00025-3
- Fung YC, Liu SQ (1989) Change of residual strains in arteries due to hypertrophy caused by aortic constriction. Circ Res 65(5):1340–1349
- Gagan JR, Tholpady SS, Ogle RC (2007) Cellular dynamics and tissue interactions of the dura mater during head development. Birth Defects Res Part C Embryo Today Rev 81(4):297–304. https:// doi.org/10.1002/bdrc.20104
- Greenwald JA, BJ Mehrara, JA Spector, SM Warren, FE Crisera, PJ Fagenholz, PJ Bouletreau, MT Longaker (2000) Regional differentiation of cranial suture-associated dura mater in vivo and in vitro: implications for suture fusion and patency. J Bone Miner Res 15 (12):2413-2430. https://doi.org/10.1359/jbmr.2000.15.12.2413.
- Gregersen H, Kassab G, Fung Y (2000) REVIEW: the zero-stress state of the gastrointestinal tract. Dig Dis Sci 45(12):2271–2281. https://doi.org/10.1023/A:1005649520386
- Han H, Fung Y (1991) Residual strains in porcine and canine trachea. J Biomech 24(5):307–315. https://doi.org/10.1016/0021-9290(91) 90349-R
- Henderson JH, Nacamuli RP, Zhao B, Longaker MT, Carter DR (2005) Age-dependent residual tensile strains are present in the dura mater of rats. J R Soc Interface 2(3):159–167. https://doi.org/10. 1098/rsif.2005.0035
- Herring SW, Teng S (2000) Strain in the braincase and its sutures during function. Am J Phys Anthropol 112(4):575. https://doi.org/10.1002/1096-8644(200008)112:4<575::AIDAJPA10>3.0.CO;2-0
- Holland MA (2018). Hitchhiker's guide to abaqus. https://doi.org/10.5281/zenodo.1243270
- Jaslow CR (1990) Mechanical properties of cranial sutures. J Biomech 23(4):313–321. https://doi.org/10.1016/0021-9290(90)90059-C
- Jimenez Hamann MC, Sacks MS, Malinin TI (1998) Quantification of the collagen fiber architecture of human cranial dura mater. J Anat 192(Pt 1):99–106. https://doi.org/10.1046/j.1469-7580. 1998.19210099.x
- Kamenskiy AV II, Pipinos YA Dzenis, Lomneth CS, Kazmi SAJ, Phillips NY, MacTaggart JN (2014) Passive biaxial mechanical properties and in vivo axial pre-stretch of the diseased human femoropopliteal and tibial arteries. Acta Biomater 10(3):1301–1313. https://doi.org/10.1016/j.actbio.2013.12.027

- Kamenskiy AV II, Pipinos YA Dzenis, Phillips NY, Desyatova AS, Kitson J, Bowen R, MacTaggart JN (2015) Effects of age on the physiological and mechanical characteristics of human femoropopliteal arteries. Acta Biomaterialia 11:304–313. https://doi.org/ 10.1016/j.actbio.2014.09.050
- Kawakami M, Yamamura KI (2008) Cranial bone morphometric study among mouse strains. BMC Evol Biol 8(1):73. https://doi.org/10. 1186/1471-2148-8-73
- Kinaci A, Bergmann W, Bleys RL, van der Zwan A, van Doormaal TP (2020) Histologic Comparison of the Dura Mater among Species. Comp Med 70 (2):170-175. https://doi.org/10.30802/AALAS CM-19-000022
- Kriewall TJ, Akkas N, Bylski DI, Melvin JW, Work BA (1983) Mechanical behavior of fetal dura mater under large axisymmetric inflation. J Biomech Eng 105(1):71–76. https://doi.org/10.1115/1. 3138388
- Kuchiwaki H, Inao S, Ishii N, Ogura Y, Gu SP (1997) Human dural thickness measured by ultrasonographic method: reflection of intracranial pressure. J Ultrasound Med 16(11):725–730. https:// doi.org/10.7863/jum.1997.16.11.725
- Laurence DW, Ross CJ, Hsu MC, Mir A, Burkhart HM, Holzapfel GA, Lee CH (2022) Benchtop characterization of the tricuspid valve leaflet pre-strains. Acta Biomaterialia. https://doi.org/10.1016/j. actbio.2022.08.046
- Liu SSY, Opperman LA, Kyung HM, Buschang PH (2011) Is there an optimal force level for sutural expansion. Am J Orthod Dentofac Orthop Off Publ Am Assoc Orthod Its Const Soc Am Board Orthod 139(4):446–455. https://doi.org/10.1016/j.ajodo.2009.03.056
- Maikos JT, Elias RA, Shreiber DI (2008) Mechanical properties of dura mater from the rat brain and spinal cord. J Neurotrauma 25(1):38–51. https://doi.org/10.1089/neu.2007.0348
- McGarvey KA, Lee JM, Boughner DR (1984) Mechanical suitability of glycerol-preserved human dura mater for construction of prosthetic cardiac valves. Biomaterials 5(2):109–117. https://doi.org/10.1016/0142-9612(84)90011-5
- Melvin JW, JH McElhaney, VL Roberts (1970). Development of a mechanical model of the human head–determination of tissue properties and synthetic substitute materials. SAE Trans 79:Publisher: SAE International, 2685-2694. ISSN: 0096-736X
- Ogle RC, Tholpady SS, McGlynn KA, Ogle RA (2004) Regulation of cranial suture morphogenesis. Cells Tissues Organs 176(1):54–66. https://doi.org/10.1159/000075027
- Opperman LA, Passarelli RW, Morgan EP, Reintjes M, Ogle RC (1995) Cranial sutures require tissue interactions with dura mater to resist osseous obliteration in vitro. J Bone Miner Res 10(12):1978– 1987. https://doi.org/10.1002/jbmr.5650101218
- O'Reilly MA, A Muller, K Hynynen (2011). Ultrasound insertion loss of rat parietal bone appears to be proportional to animal mass at sub-megahertz frequencies. Ultrasound Med Biol 37 (11):1930-1937. https://doi.org/10.1016/j.ultrasmedbio.2011.08.001.
- Patin DJ, Eckstein EC, Harum K, Pallares VS (1993) Anatomic and biomechanical properties of human lumbar dura mater. Anesth Analgesia 76(3):535–540
- Pierrat B, Carroll L, Merle F, MacManus DB, Gaul R, Lally C, Gilchrist MD, Ní Annaidh A (2020) Mechanical characterization and modeling of the porcine cerebral meninges. Front Bioeng Biotechnol 8:801. https://doi.org/10.3389/fbioe.2020.00801
- Protasoni M, Sangiorgi S, Cividini A, Culuvaris GT, Tomei G, Dell'Orbo C, Raspanti M, Balbi S, Reguzzoni M (2011) The collagenic architecture of human dura mater: laboratory investigation. J Neurosurg 114(6):1723–1730. https://doi.org/10.3171/2010.12.JNS101732
- Rasband WS (2018) ImageJ. Bethesda, Maryland, USA



- Rausch MK, Kuhl E (2013) On the effect of prestrain and residual stress in thin biological membranes. J Mech Phys Solids 61(9):1955–1969. https://doi.org/10.1016/j.jmps.2013.04.005
- Richtsmeier JT, Flaherty K (2013) Hand in glove: brain and skull in development and dysmorphogenesis. Acta Neuropathol 125:469–489. https://doi.org/10.1007/s00401-013-1104-y
- Rodriguez EK, Hoger A, McCulloch AD (1994) Stress-dependent finite growth in soft elastic tissues. J Biomech 27(4):455–467. https:// doi.org/10.1016/0021-9290(94)90021-3
- Shulyakov AV, Cenkowski SS, Buist RJ, Del Bigio MR (2011) Agedependence of intracranial viscoelastic properties in living rats. J Mech Behav Biomed Mater 4(3):484–497. https://doi.org/10. 1016/j.jmbbm.2010.12.012
- Suh DC (2020) Where Did the dura mater come from. Neurointervention 15(1):2–3. https://doi.org/10.5469/neuroint.2020.00045
- van Noort R, Black MM, Martin TRP, Meanley S (1981) A study of the uniaxial mechanical properties of human dura mater preserved in glycerol. Biomaterials 2(1):41–45. https://doi.org/10.1016/0142-9612(81)90086-7
- Vandenabeele F, Creemers J, Lambrichts I (1996) Ultrastructure of the human spinal arachnoid mater and dura mater. J Anat 189(Pt 2):417–430
- Weickenmeier J, Fischer C, Carter D, Kuhl E, Goriely A (2017) Dimensional, geometrical, and physical constraints in skull growth. Phys Rev Lett 118(24):248101
- Weiss-Bilka HE, Brill JA, Ravosa MJ (2018) Non-sutural basicranium-derived cells undergo a unique mineralization pathway via a cartilage intermediate in vitro. PeerJ 6:e5757. https://doi.org/10.7717/peerj.5757
- Wolfinbarger L Jr, Zhang Y, Adam BLT, Homsi D, Gates K, Sutherland V (1994) Biomechanical aspects on rehydrated freeze-dried human allograft dura mater tissues. J Appl Biomater 5(3):265–270. https://doi.org/10.1002/jab.770050313

- Woolrich MW, Jbabdi S, Patenaude B, Chappell M, Makni S, Behrens T, Beckmann C, Jenkinson M, Smith SM (2009) Bayesian analysis of neuroimaging data in FSL. NeuroImage 45(1):S173–S186. https://doi.org/10.1016/j.neuroimage.2008.10.055
- Workman AD, Charvet CJ, Clancy B, Darlington RB, Finlay BL (2013) Modeling Transformations of Neurodevelopmental Sequences across Mammalian Species. J Neurosci 33(17):7368–7383. https://doi.org/10.1523/JNEUROSCI.5746-12.2013
- Xu G, Bayly PV, Taber LA (2009) Residual stress in the adult mouse brain. Biomech Model Mechanobiol 8(4):253–262. https://doi.org/10.1007/s10237-008-0131-4
- Yamaki T, Uede T, Tano-oka A, Asakura K, Tanabe S, Hashi K (1991)
 Vascularized omentum graft for the reconstruction of the skull
 base after removal of a nasoethmoidal tumor with intracranial
 extension: case report. Neurosurgery 28(6):877–880. https://doi.
 org/10.1097/00006123-199106000-00015
- Yu JC, Buchman SR, Gosain AK, Havlik RJ, Wang TH, Lam PS, Masoumy M (2021) Basic biomechanics for craniofacial surgeons: the responses of alloplastic materials and living tissues to mechanical forces. FACE 2(4):446–461
- Zwirner J, Scholze M, Waddell JN, Ondruschka B, Hammer N (2019) Mechanical properties of human dura mater in tension–an analysis at an age range of 2 to 94 years. Sci Reports 9(1):16655. https:// doi.org/10.1038/s41598-019-52836-9

Springer Nature or its licensor (e.g. a society or other partner) holds exclusive rights to this article under a publishing agreement with the author(s) or other rightsholder(s); author self-archiving of the accepted manuscript version of this article is solely governed by the terms of such publishing agreement and applicable law.

